Journal of ELECTRONIC MATERIALS, Vol. 45, No. 8, 2016
DOI: 10.1007/s11664-016-4635-x

Effect of Substitution of Mn, Cu, and Zr on the Structural, Magnetic, and Ku-Band Microwave-Absorption Properties of Strontium Hexaferrite Nanoparticles

MOHAMMAD ROSTAMI,[1] MAHMOOD MORADI,[1,2,4] REZA SHAMS ALAM,[1] and REZA MARDANI[3]

1.—Physics Department, College of Sciences, Shiraz University, Shiraz 71946-84795, Iran. 2.—Institute of Nanotechnology, Shiraz University, Shiraz 71454, Iran. 3.—Air-Nautical Research Center, Shiraz 71946-84043, Iran. 4.—e-mail: moradi@susc.ac.ir

The ferrites with the compositions of $SrMn_xCu_xZr_{2x}Fe_{(12-4x)}O_{19}$ (x = 0.0, 0.2, 0.3, 0.4, and 0.5) are synthesized by the coprecipitation method. The formation of *M*-type hexaferrite is confirmed by x-ray diffraction (XRD) and Fourier transform infrared (FTIR) analyses. The morphology of the samples is shown by field emission scanning electron microscopy (FESEM) and transmission electron microscopy (TEM) microscopy. Vibrating sample magnetometer (VSM) analysis has been used for the investigation of the magnetic properties, and the reason for the changes in the magnetic properties as a result of doping, are expressed. The values of coercivity decrease by increasing the amount of substitution, which could be related to the modification of anisotropy form the *c*-axis toward the *c*-plane. Finally, we have used vector network analysis to investigate the microwave absorption properties. We find that the samples with the composition of $SrMn_{0.4}Cu_{0.4}Zr_{0.8}Fe_{10.4}O_{19}$ have the largest reflection loss and the widest bandwidth among these samples.

Key words: Magnetic materials, strontium hexaferrite, magnetic properties, reflection loss, microwave absorbers

INTRODUCTION

Recently, we have observed so many advances in the field of microwave and antenna technology.[1,2] However, by the improvement of microwave devices and the development of the microwave applications in our lives, the need for the materials that can absorb the electromagnetic waves increases. We can use these kinds of materials especially for two purposes. First, these materials can prevent the electromagnetic waves from disturbing the parts of the microwave devices or other devices that are subject to electromagnetic waves. Second, electromagnetic radiation may be harmful to living organisms, and we can use these kinds of materials to preserve them from suffering from electromagnetic radiation.

(Received February 14, 2016; accepted May 5, 2016; published online May 25, 2016)

One kind of electromagnetic wave absorbers is strontium hexaferrite with the chemical formula of $SrFe_{12}O_{19}$ (SrM). The appropriate properties of this material such as low cost and high stability cause it to be a good candidate in order to be used as an electromagnetic wave absorber.[3,4] The reflection loss of this material could be improved by the substitution of some of the transition metal elements for iron atoms.[5] We can also shift the reflection loss peak to the desired frequencies by this procedure.[6]

In this paper, we have used Mn, Cu, and Zr as our dopants for strontium hexaferrite. The chemical formula of the nanoparticles is $SrMn_xCu_xZr_{2x}Fe_{12-4x}O_{19}$ (x = 0.0, 0.2, 0.3, 0.4, and 0.5). We find that the saturation magnetization and the coercivity are decreased by increasing the dopant concentration of the samples. However, the reflection loss is improved by increasing the dopant concentration. It is found that the samples with the chemical

composition of $SrMn_{0.4}Cu_{0.4}Zr_{0.8}Fe_{10.4}O_{19}$ have the lowest reflection loss minimums and the widest bandwidth among these samples.

EXPERIMENTAL PROCEDURE

The nanoparticles were synthesized via the chemical coprecipitation method. First, the stoichiometric amounts of $ZrO(NO_3)_2{\cdot}xH_2O$, $MnCl_2{\cdot}4H_2O$, $CuCl_2{\cdot}2H_2O$, $FeCl_3$, and $SrCl_2.6H_2O$ were put in a sufficient amount of deionized water at 70°C and stirred for 20 min to form a homogenous solution. Next, 2 wt.% of surfactant (polyvinyl alcohol (PVA)) was also added to the solution. Then, 1.5 M NaOH solution was added dropwise to the solution, and the pH level was adjusted to 13. The resulted precipitates were washed and filtered for several times until a solution with a pH value of 7 was achieved. Finally, the precipitates were dried at 90°C and calcined at 900°C for 2 h.

The structural properties of the samples were investigated using x-ray diffraction (XRD) spectroscopy with Cu-Kα radiation. Fourier transform infrared (FTIR) spectroscopy was done to identify the nature of the chemical bonds. After that, field emission scanning electron microscopy (FESEM) and transmission electron microscopy (TEM) were used for investigating the morphology of the samples. The magnetic properties of the samples were also measured by a vibrating sample magnetometer (VSM). A vector network analyzer was used to investigate the reflection loss of the samples in the frequency range of 12–18 GHz. For this purpose, the composites specimens were prepared by mixing the prepared samples with epoxy resin with a weight percentage of 70:30, and pressing them to form cylindrical shapes with a diameter of 3 cm and a thickness of 2 mm.

RESULTS AND DISCUSSION

Structural Properties

First, we obtained the XRD spectra of the samples. Figure 1 shows the XRD patterns of $SrMn_xCu_xZr_{2x}Fe_{12-4x}O_{19}$ (x = 0.0, 0.2, 0.3, 0.4, and 0.5) nanoparticles. From this figure, we find that all of the transition-metal-substituted ferrites have almost a single phase structure of M type.

The lattice parameters of the samples have been calculated from the obtained XRD patterns using the following relations:

$$\frac{1}{d^2} = \frac{4}{3}\frac{h^2 + kh + k^2}{a^2} + \frac{l^2}{c^2}, \quad (1)$$

$$n\lambda = 2d\sin\theta. \quad (2)$$

In these relations, a and c are the hexagonal lattice parameters, d is the difference between successive surfaces, n is an integer, λ is the wavelength of the x-ray (1.54 Å), and θ is the Bragg angle. The crystallite sizes of the particles were also calculated using the Scherrer equation[7]:

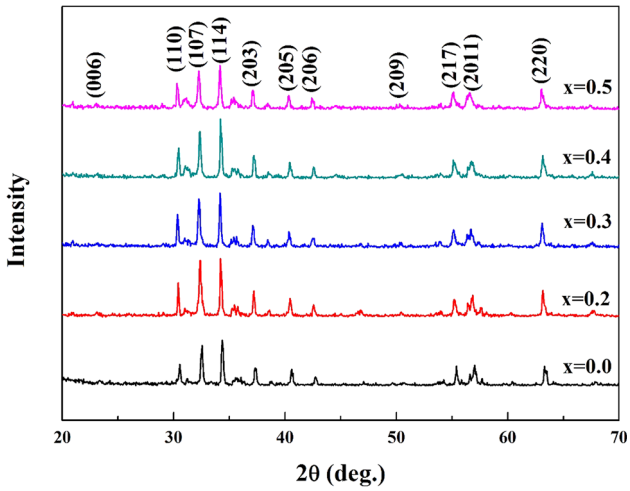

Fig. 1. The XRD patterns of $SrMn_xCu_xZr_{2x}Fe_{12-4x}O_{19}$ (x = 0.0, 0.2, 0.3, 0.4, and 0.5) nanoparticles.

$$D = \frac{k\lambda}{\beta\cos\theta}, \quad (3)$$

where β is the broadening of diffraction line at half of its maximum intensity, and k is the shape factor, which is equal to 0.89 for hexagonal systems.

The lattice parameters (a and c), cell volume (v), and crystallite size (D) of the samples are listed in Table I. We can see from this table that the crystallite sizes of the samples are in the range of 41.74–41.77 nm. Figure 2 shows the variation of a and c lattice constants with doping concentration (x). It is clear from this figure that the lattice constant a remains almost constant while c increases from 22.91 Å to 23.11 Å with increasing the dopant concentration. These changes in the lattice parameters can be related to the larger ionic radius of Mn^{+2} (0.80 Å), Zr^{+4} (fourfold 0.73 Å and sixfold 0.86 Å) and Cu^{+2} (fourfold 0.74 Å and sixfold 0.91 Å) compared to the ionic radius of Fe^{+3} (0.69 Å).

FTIR spectroscopy has been used to identify the nature of the chemical bonds. Figure 3 represents the FTIR spectra of the $SrMn_xCu_xZr_{2x}Fe_{12-4x}O_{19}$ (x = 0.0, 0.2, 0.3, 0.4, and 0.5). We can see two peaks in the range between 400 cm^{-1} and 800 cm^{-1} for all of the samples, which are related to the Fe–O stretching vibrational band in octahedral and tetrahedral sites.[8–10] The substitution of Mn^{+2}, Cu^{+2} and Zr^{+4} atoms lead to the shift of the peaks toward the low frequency side. There is an absorption peak at about 547 cm^{-1} in the undoped sample (x = 0.0), which is assigned to Sr–O bond.[11] We cannot see the same peak in other spectra, because of the shift of the bands toward low frequency side with the increase of dopant contents. The peaks in the range of 1100–1500 cm^{-1} are assigned to M–O–M (metal–oxygen–metal) bonds such as Fe–O–Fe bonds. The

Table I. The lattice constants *a* and *c*, the cell volume *v*, and the crystallite size *D* of $SrMn_xCu_xZr_{2x}Fe_{12-4x}O_{19}$ (x = 0.0, 0.2, 0.3, 0.4, and 0.5)

x	*a* (Å)	*c* (Å)	*v* (Å^3)	*D* (nm)
0.0	5.85	22.91	678.99	41.77
0.2	5.86	23.02	684.59	41.76
0.3	5.87	23.07	688.42	41.75
0.4	5.87	23.09	689.02	41.75
0.5	5.88	23.11	691.97	41.74

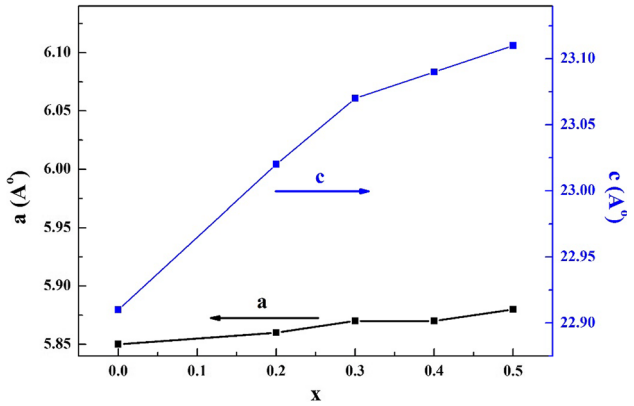

Fig. 2. The variation of *a* and *c* lattice constants with doping concentration (x) for $SrMn_xCu_xZr_{2x}Fe_{12-4x}O_{19}$ (x = 0.0, 0.2, 0.3, 0.4, and 0.5).

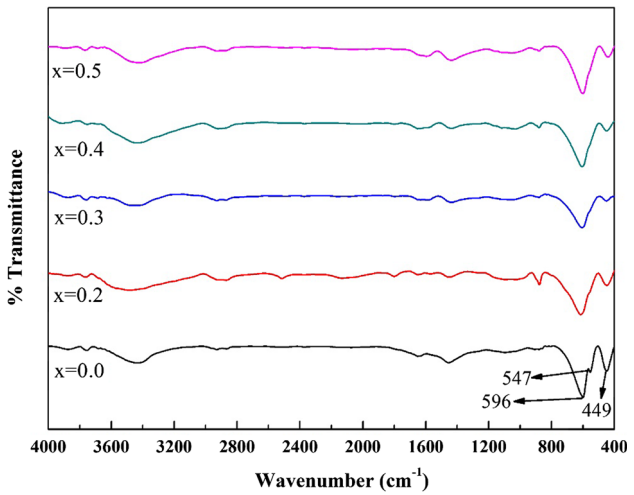

Fig. 3. The FTIR spectra of $SrMn_xCu_xZr_{2x}Fe_{12-4x}O_{19}$ (x = 0.0, 0.2, 0.3, 0.4, and 0.5) nanoparticles.

peaks around 3400 cm^{-1} in all of the spectra exhibit the –OH stretching vibrational band, which are acquired from a wet atmosphere.

The FESEM images of the $SrMn_xCu_xZr_{2x}Fe_{12-4x}O_{19}$ (x = 0.0, 0.2, 0.3, 0.4, and 0.5) nanoparticles are given in Fig. 4. We can see that the ferrite nanoparticles possess irregular shapes with both fine and large nanoparticles, and the particles are agglomerated due to the magnetic nature of them. As it is clear from this figure, the particles are platelet in shape for the undoped samples with a thickness of less than 50 nm. However, by increasing the dopant concentration, the number of platelet-like particles, which are as long as the size of the particles, are decreased and that is related to the pH of the precursors.[11,12] When we increase the concentration of dopants, the pH of the solvent decreases, and as a result, a higher amount of NaOH is needed to achieve the suitable pH of 13. Therefore, the nucleation rate of precipitation increases, which may lead to a decrease in the particle size.[12]

Since the particles shown in the FESEM micrographs are agglomerated, and we cannot specify the exact sizes of the particles, we also present the TEM image for one of the samples. This image for $SrFe_{12}O_{19}$ nanoparticle is presented in Fig. 5. The average value of the particle size calculated by TEM is found to be about 80 nm.

Magnetic Properties

The magnetic properties of the samples have been investigated using VSM analysis. Figure 6 presents the hysteresis loops for $SrMn_xCu_xZr_{2x}Fe_{12-4x}O_{19}$ (x = 0.0, 0.2, 0.3, 0.4, and 0.5) compounds. We can see from these figures that doping with transition elements can affect the magnetic properties of the samples. We find that the value of saturation magnetization (M_s) increases up to x = 0.2 and then decreases slowly with the increase in the amount of doping. However, the values of coercivity (H_c) and remanence (M_r) are reduced by increasing the concentration of dopant ions.

There are five crytallographically inequivalent sites for the twelve Fe^{+3} ions in strontium hexaferrite crystal structure, which are known as 4f$_1$, 4f$_2$, 12k, 2a, and 2b sites. The Fe^{+3} ions have spin-up direction in the 12k, 2a, and 2b sites, and they havea spin-down direction in the 4f$_1$ and 4f$_2$ sites. The magnetic moment of Fe^{+3} is 5μ_B which is equal to the magnetic moment of Mn^{+2} and is larger than the magnetic moments of Cu^{+2} (1μ_B) and Zr^{+4} (nonmagnetic). It is found that Zr^{+4} prefers to occupy 4f$_1$ sites,[13] and Cu^{+2} ions have a preference for the octahedral sites (2a, 12 k and 4f$_2$ sites).[14] It seems that for a low concentration of the dopants (x = 0.2), the substitution of the Fe^{+3} ions in the 4f$_1$ sites that have downward spin direction by the nonmagnetic Zr^{+4} ions increases the saturation magnetization of the sample. However, the saturation magnetization (M_s) and remanence (M_r) decrease with further increase in the dopant concentrations. The substitutions of Cu^{+2} ions for Fe^{+3} ions in octahedral sites of 2a and 12 k would reduce the saturation magnetization because Fe^{+3} in these sites have a spin-up direction. In addition, the substitutions of nonmagnetic Zr^{+4} and less magnetic Cu^{+2} ions for Fe^{+3} ions in 4f$_1$ and the octahedral site

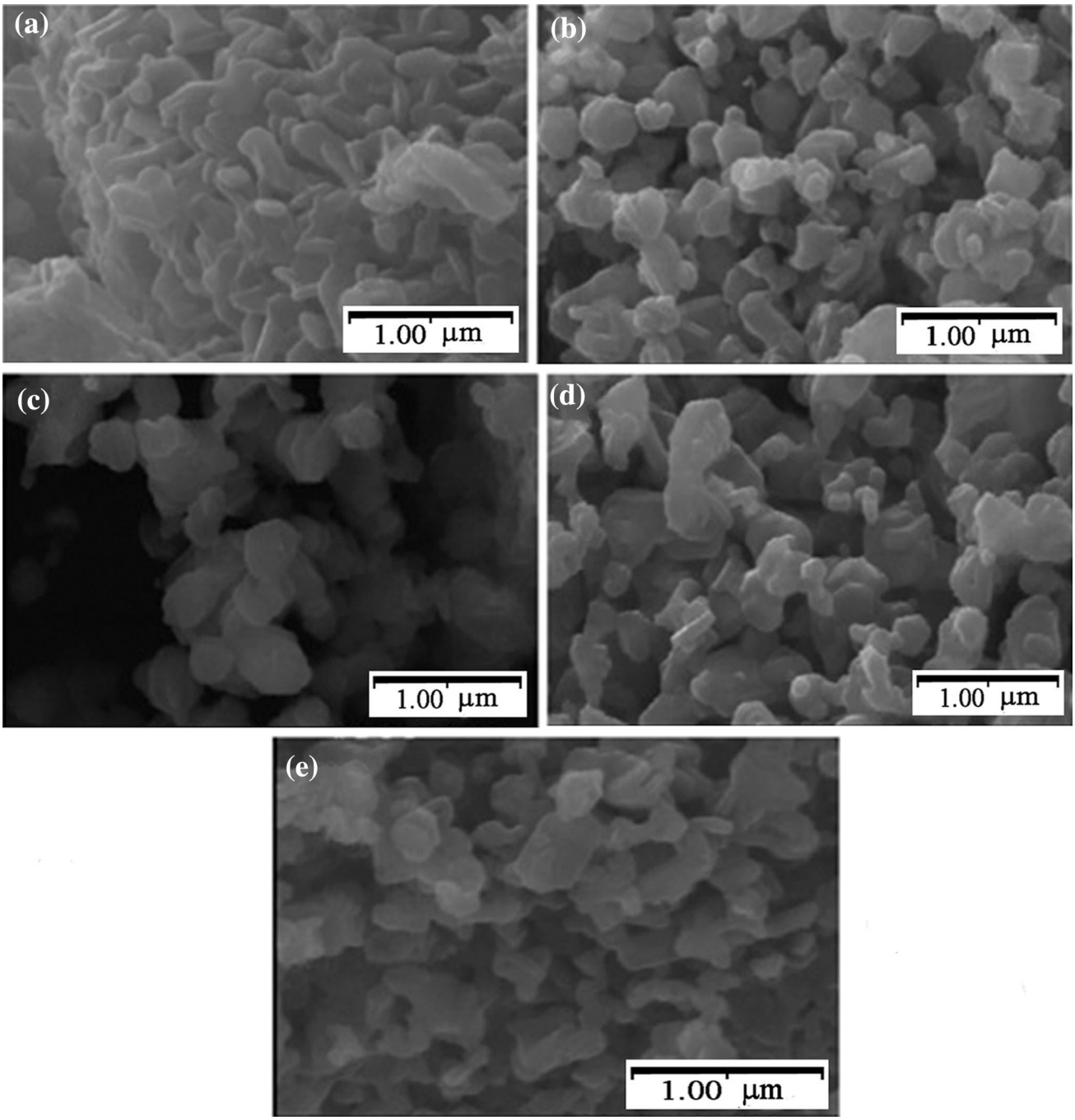

Fig. 4. The FESEM images of $SrMn_xCu_xZr_{2x}Fe_{12-4x}O_{19}$ nanoparticles for (a) $x = 0.0$, (b) $x = 0.2$, (c) $x = 0.3$, (d) $x = 0.4$, and (e) $x = 0.5$.

of $4f_2$ can also reduce the superexchange interactions between these sites and other sites with a spin-up direction, which may change the spin direction of Fe^{+3} ions in these sites. This can reduce the saturation magnetization of the samples with higher concentrations of dopants.

We can also see from Fig. 6 that the coercivity decreases continuously by increasing the doping concentration of the samples. There are two reasons for the reduction in the coercivity of the nanoparticles. First, as mentioned earlier, doping of the samples increases the lattice constant *c,* which may reduce the superexchange interactions between neighboring ions. Second, this reduction in coercivity occurs due to a reduction in magnetocrystalline anisotropy of the samples. It is found that the Fe^{+3} ions in the $4f_2$ and 2b sites have the main contribution to the magnetocrystalline anisotropy, although the contribution of the Fe^{+3} ions in other sites are not negligible.[15–17] As mentioned above,

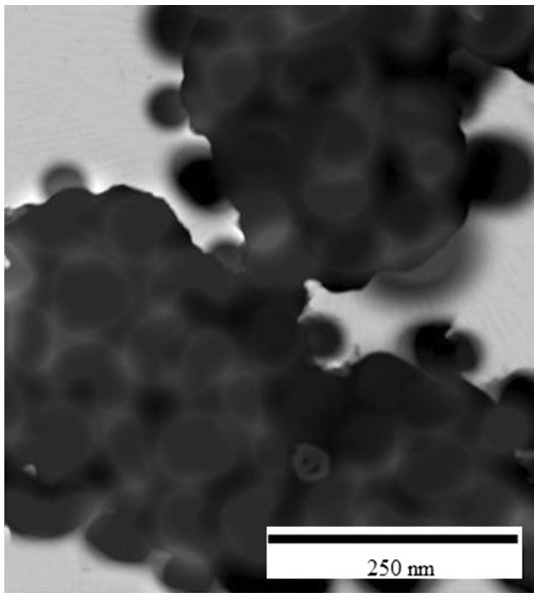

Fig. 5. The TEM images of $SrFe_{12}O_{19}$ nanoparticles.

Cu^{+2} ions have a preference to occupy the octahedral sites that can decrease the magnetocrystalline anisotropy. In addition, the substitution of Fe^{+3} ions in $4f_1$ sites by Zr^{+4} ions has a negative impact on the magnetocrystalline anisotropy.[15,17] Generally, it could be inferred from the obtained results that the anisotropy, and as a result, coercivity of the samples could be controlled by substitution. In fact, substitution, which leads to the modification of anisotropy form the *c*-axis toward the *c*-plane, plays a key role in decreasing the value of coercivity.[16,18]

Microwave Absorption Properties

The microwave absorption properties of the samples are obtained byvector network analysis. Figure 7 shows the absorption diagrams of the samples in the frequency range of 12–18 GHz (Ku band frequencies). The resonance frequency of the undoped strontium hexaferrite was found to be 48 GHz that is larger than the Ku band frequencies.[19] This rather high resonance frequency is related to the high magnetocrystalline anisotropy of the undoped strontium hexaferrite.

According to the ferromagnetic resonance theory, the resonance frequency (f_r) of the samples is related to the anisotropy field (H_a) as given by the following equation:

$$f_r = \frac{\gamma}{2\pi} H_a, \tag{4}$$

where γ is the gyromagnetic ratio. In the case of uniaxial anisotropy, H_a is given as follows:

$$H_a = \frac{2K_1}{M_s}, \tag{5}$$

where M_s is the saturation magnetization and K_1 is the anisotropy constant. Findings of the present study proved that the coercivity decreases by increasing the amount of substitution of Mn-Cu-Zr cations for Fe^{+3} ions in the hexaferrite structure. Also, it is well known that coercivity is closely related to the anisotropy field.[16,20,21] Hence, according to Eq. 4, an increase in the amount of substitution causes the resonance frequency to shift to a lower frequency range. The variations of the reflection loss versus frequency for the samples with different amounts of substitutions are presented in Fig. 7.

As we can see from Fig. 7, there is no considerable absorption for the undoped strontium hexaferrite (x = 0.0). However, it seems that the resonance frequencies are moved to the Ku band as we add the dopants to the compounds. Here, the bandwidth is defined as the frequency width in which the reflection loss is higher than −20 dB. The sample with the composition of $SrMn_{0.2}Cu_{0.2}Zr_{0.4}Fe_{11.2}O_{19}$ has a bandwidth of zero, and the minimum reflection loss is −15.29 dB at the matching frequency of 14.20 GHz. There is also another matching frequency at 16.44 GHz with the reflection loss of −13.02 dB. We can also see the same features for the other doped samples so that we can see two absorption peaks, one at a low frequency range and the other at a high frequency range. The absorption at the low frequency is related to the domain wall motion, and the one at the high frequency is due to the natural resonance frequency.[9,10,22] The sample with the composition of $SrMn_{0.3}Cu_{0.3}Zr_{0.6}Fe_{10.8}O_{19}$ has a bandwidth of 0.205 GHz, and the minimum reflection loss is −22.11 dB at the matching frequency of 14.14 GHz. The ferrite with the composition of $SrMn_{0.4}Cu_{0.4}Zr_{0.8}Fe_{10.4}O_{19}$ has a bandwidth of 5.11 GHz and the minimum reflection loss of −31.23 dB at the matching frequency of 13.87 GHz. The minimum of the reflection loss for $SrMn_{0.5}Cu_{0.5}ZrFe_{10}O_{19}$ is −30.97 dB at the matching frequency of 14.01 GHz with the bandwidth of 4.48 GHz. Comparing these results, we find that the sample with the composition of $SrMn_{0.4}Cu_{0.4}Zr_{0.8}Fe_{10.4}O_{19}$ has the widest bandwidth and the largest reflection loss. A suitable microwave absorbing material should have wide frequency bandwidth and large reflection loss.[23] Therefore, among these samples, the nanoparticles with the composition of $SrMn_{0.4}Cu_{0.4}Zr_{0.8}Fe_{10.4}O_{19}$ are the most appropriate microwave absorbing material. Although the minimum reflection losses lower than the ones obtained for our samples were reported previously, the bandwidths of our samples are much wider than those, which means that our samples could be applied for a wider range of frequency.

In general, for preparing a potential microwave absorber in the desired frequency range, two important conditions must be satisfied, the first is that the incident wave can enter the absorber to the greatest

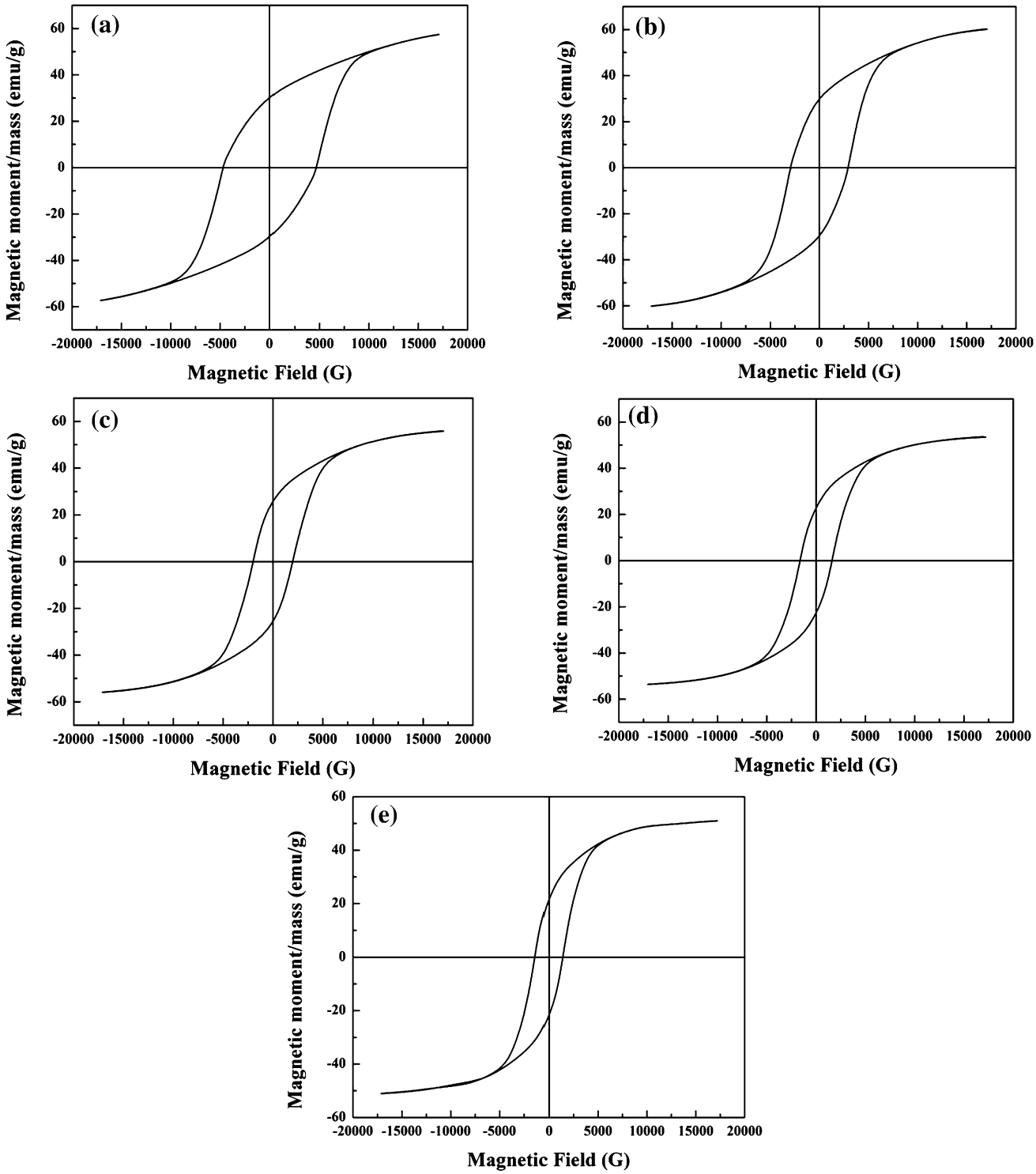

Fig. 6. Hysteresis loops of $SrMn_xCu_xZr_{2x}Fe_{12-4x}O_{19}$ nanoparticles for (a) $x = 0.0$, (b) $x = 0.2$, (c) $x = 0.3$, (d) $x = 0.4$, and (e) $x = 0.5$.

extent (impedance matching characteristic), and the second is that the electromagnetic wave entering into the materials can be almost entirely attenuated and absorbed within the finite thickness of the absorber (attenuation characteristic). To this end, saturation magnetization, anisotropy field, complex permittivity, and permeability spectra are among the most important parameters which should be of concern in designing a microwave absorber. It should be mentioned that these parameters could be easily controlled by substituting Fe^{+3} ions by other cations in the hexaferrite structure. Particle

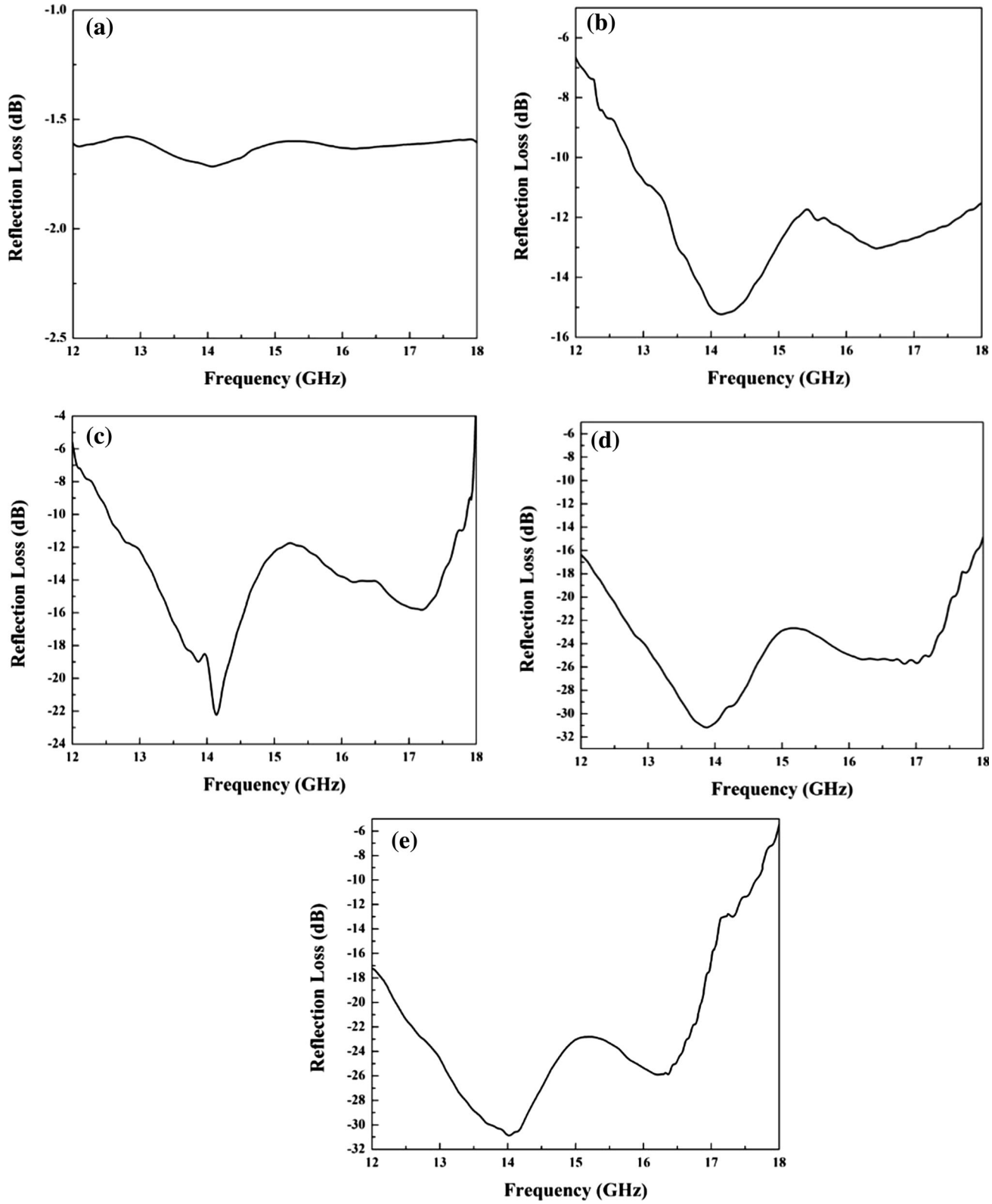

Fig. 7. The microwave absorption diagrams of $SrMn_xCu_xZr_{2x}Fe_{12-4x}O_{19}$ nanoparticles for (a) $x = 0.0$, (b) $x = 0.2$, (c) $x = 0.3$, (d) $x = 0.4$, and (e) $x = 0.5$.

size is another key issue that influences the microwave absorbing performance. In general, when the particle size is reduced, the quantum confinement and surface effects can change the microwave absorption properties of the samples significantly. Quantum confinement leads to the

splitting of the energy levels in the nanoparticles, and the electrons can absorb the energy of microwaves and go to higher energy levels that lead to more energy absorption of microwaves.[8,24] Breaking of the bonds at the surfaces causes the surface spins to be in a disordered state that may lead to high magnetic losses in the samples. The defects and interfaces can also result in multiple scattering and the repetition of the reflection of the incident wave between nanoparticles that increases the reflection loss of the compounds.

SUMMARY AND CONCLUSIONS

The nanoparticles of strontium hexaferrite doped with Mn, Cu, and Zr with different concentration of dopants were synthesized by the coprecipitation method. The XRD and FTIR analyses show that all of the samples are in the *M*-type hexaferrite structure with the crystallite size of about 41.7 nm. From the FESEM micrographs, it was found that ferrite particles have irregular shapes, and the size of the particles decreases by increasing the dopant concentration. We also found from TEM analysis that the average particle size is about 80 nm. VSM analysis has been used to consider the magnetic properties of the samples. It was found that, by increasing the concentration of dopants, the saturation magnetization initially increased and then decreased; however, the remanence and coercivity decreased continuously by adding dopants. The reasons for these changes were also expressed. The microwave absorption properties of the samples were also obtained by vector network analysis. We found that doping of the samples causes the resonance frequency to decrease, and the sample with the composition of $SrMn_{0.4}Cu_{0.4}Zr_{0.8}Fe_{10.4}O_{19}$ has the largest reflection loss and the widest bandwidth of 5.11 GHz which is much larger than the ones that were reported previously.

REFERENCES

1. G.R. Gordani, A. Ghasemi, and A. Saidi, *J. Magn. Magn. Mater.* 391, 184 (2015).
2. R. Shams Alam, M. Moradi, M. Rostami, H. Nikmanesh, R. Moayedi, and Y. Bai, *J. Magn. Magn. Mater.* 381, 1 (2015).
3. V. Bilovol and R. Martínez-García, *J. Phys. Chem. Solids* 86, 131 (2015).
4. M. Mousavinia, A. Ghasemi, and E. Paimozd, *J. Electron. Mater.* 42, 2784 (2013).
5. C.L. Yuan and Y.S. Tuo, *J. Magn. Magn. Mater.* 342, 47 (2013).
6. M. Jamalian, A. Ghasemi, and E. Paimozd, *J. Alloys Compd.* 604, 373 (2014).
7. B.D. Cullity, *Elements of X-ray Powder Diffraction* (Cambridge, MA: Addison-Wesley Publishing Company, 1978).
8. G.R. Gordani, A. Ghasemi, and A. Saidi, *Ceram. Int.* 40, 4945 (2014).
9. A. Baniasadi, A. Ghasemi, A. Nemati, M.A. Ghadikolaei, and E. Paimozd, *J. Alloys Compd.* 583, 325 (2014).
10. S.K. Chawla, R.K. Mudsainiyan, S.S. Meena, and S.M. Yusuf, *J. Magn. Magn. Mater.* 350, 23 (2014).
11. A. Davoodi and B. Hashemi, *J. Alloys Compd.* 509, 5893 (2011).
12. R. Shams Alam, M. Moradi, H. Nikmanesh, J. Ventora, and M. Rostami, *J. Magn. Magn. Mater.* 402, 20 (2016).
13. M.N. Ashiq, M.J. Iqbal, and I.H. Gul, *J. Alloys Compd.* 487, 341 (2009).
14. B.X. Gu, *J. Appl. Phys.* 74, 1247 (1993).
15. S.Y. An, I.B. Shim, and C.S. Kim, *J. Appl. Phys.* 91, 8465 (2002).
16. E. Kiani, A.S.H. Rozatian, and M.H. Yousefi, *J. Magn. Magn. Mater.* 361, 25 (2014).
17. Z. Yang, C.S. Wang, X.H. Li, and H.X. Zeng, *Mater. Sci. Eng.* 90, 142 (2002).
18. L. Wang, H. Yu, X. Ren, and G. Xu, *J. Alloys Compd.* 588, 212 (2014).
19. F. Tabatabaie, M.H. Fathi, A. Saatchi, and A. Ghasemi, *J. Alloys Compd.* 474, 206 (2009).
20. M. Awawdeh, I. Bsoul, and S.H. Mahmood, *J. Alloys Compd.* 585, 465 (2014).
21. A.M. Alsmadi, I. Bsoul, S.H. Mahmood, G. Alnawashi, F.M. Al-Dweri, Y. Maswadeh, and U. Welp, *J. Alloys Compd.* 648, 419 (2015).
22. S. Choopani, N. Keyhan, A. Ghasemi, A. Sharbati, and R. Shams Alam, *Mater. Chem. Phys.* 113, 717 (2009).
23. N. Chen, K. Yang, and M.Y. Gu, *J. Alloys Compd.* 490, 609 (2010).
24. A. Kawabata and R. Kubo, *J. Phys. Soc. Jpn.* 21, 1765 (1966).